Experimental constraints on Li isotope fractionation during the interaction between kaolinite and seawater

Xu (Yvon) Zhang, Giuseppe D. Saldi, Jacques Schott, Julien Bouchez, Marie Kuessner, Y. Montouillout, Michael J. Henehan, Jerome Gaillardet

HAL Id: insu-03033594

https://insu.hal.science/insu-03033594

Submitted on 9 Dec 2021

Journal Pre-proofs

Experimental constraints on Li isotope fractionation during the interaction between kaolinite and seawater

Xu (Yvon) Zhang, Giuseppe D. Saldi, Jacques Schott, Julien Bouchez, Marie Kuessner, Valérie Montouillout, Michael Henehan, Jérôme Gaillardet

Please cite this article as: (Yvon) Zhang, X., Saldi, G.D., Schott, J., Bouchez, J., Kuessner, M., Montouillout, V., Henehan, M., Gaillardet, J., Experimental constraints on Li isotope fractionation during the interaction between kaolinite and seawater, *Geochimica et Cosmochimica Acta* (2020), doi: https://doi.org/10.1016/j.gca.2020.09.029

This is a PDF file of an article that has undergone enhancements after acceptance, such as the addition of a cover page and metadata, and formatting for readability, but it is not yet the definitive version of record. This version will undergo additional copyediting, typesetting and review before it is published in its final form, but we are providing this version to give early visibility of the article. Please note that, during the production process, errors may be discovered which could affect the content, and all legal disclaimers that apply to the journal pertain.
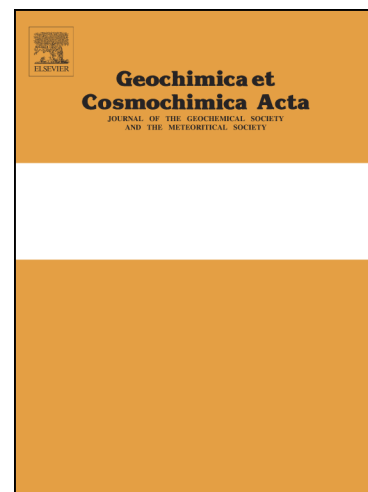
Experimental constraints on Li isotope fractionation during the interaction between kaolinite and seawater

Xu (Yvon) Zhang[a,e*], Giuseppe D. Saldi[b], Jacques Schott[b], Julien Bouchez[a], Marie Kuessner[a], Valérie Montouillout[c], Michael Henehan[d] , and Jérôme Gaillardet[a]

[a]Institut de physique du globe de Paris, Université de Paris, CNRS, 75005-F Paris, France

[b]Géosciences Environnement Toulouse, CNRS-UPS-OMP, 14 av. Édouard Belin, 31400 Toulouse, France

[c]CEMHTI CNRS UPR 3079, Université d'Orléans, 45071 Orléans Cedex 1 France

[d]Deutsches GeoForschungsZentrum GFZ, Section 3.3 Earth Surface Geochemistry, Telegrafenberg, 14473 Potsdam, Germany

[e]Laboratoire d'Hydrologie et Géochimie de Strasbourg LHyGeS, Université de Strasbourg et CNRS, 1 rue Blessig, 67084, Strasbourg Cedex, France

Corresponding author email: xuzhang@email.com

Abstract

In this study, to better understand the factors controlling the concentration and isotope composition of lithium (Li) in the ocean, we investigated the behaviour of Li during interaction of kaolinite with artificial seawater. Dissolution of kaolinite in Li-free seawater at acidic conditions (exp. 1) results in a strong preferential release of light Li isotopes, with $\Delta^7\text{Li}_{\text{aq-kaol}} \sim$ -19 ‰, likely reflecting both the preferential breaking of $^6\text{Li-O}$ bonds over $^7\text{Li-O}$ bonds and the release of Li from the isotopically lighter AlO_6 octahedral sites. Sorption experiments on kaolinite (exp. 2) revealed a partition coefficient between kaolinite and fluid of up to 28, and

an isotopic fractionation of -24 ‰. Thermodynamic calculation indicates authigenic smectites formed from the dissolution of kaolinite in seawater at pH 8.4 (exp. 3). The formation of authigenic phase strongly removed Li from the solution (with a partition coefficient between the solid and the fluid equal to 89) and led to an increase of ca. 25‰ in seawater δ^7Li. This fractionation can be described by a Rayleigh fractionation model at the early stage of the experiment during rapid clay precipitation, followed, at longer reaction time, by equilibrium isotope fractionation during the much slower removal of aqueous Li via co-precipitation and adsorption. Both processes are consistent with a fractionation factor between the solid and the aqueous solution of ~ -20‰. These experiments have implications for interpreting the Li isotopic composition of both continental and marine waters. For instance, the preferential release of ^6Li observed during kaolinite far-from-equilibrium dissolution could explain the transient enrichments in ^6Li observed in soil profiles. With regard to the evolution of seawater δ^7Li over geological time scales, our experimental results suggest that detrital material discharged by rivers to the ocean and ensuing "reverse chemical weathering" have the potential to strongly impact the isotopic signature of the ocean through the neoformation of clay minerals.

1. Introduction

The formation of authigenic clay minerals during early sedimentary diagenesis was proposed in the sixties as an important control on the concentration of major cations in the oceans (Mackenzie and Garrels, 1966; Sillen, 1967). According to this hypothesis, dissolved Na, K, and Mg are removed from seawater by interaction with suspended clays derived from continental weathering and erosion, leading to the consumption of alkalinity and to the release of acidity (CO_2). Being the opposite of a weathering reaction on the continents, this process was termed as "reverse weathering". More recently, reverse weathering has been suggested to be a key control on marine pH and climate over Earth history (Isson and Planavsky, 2018).

More than half a century after the term "reverse weathering" was first coined, however, we are still lacking key quantitative constraints on this potentially major oceanic sink. This is in part due to the challenges inherent in addressing this question experimentally, which include the slow kinetics of the processes involved and the similarity in mineralogy and chemistry between authigenic clays and allochthonous detrital clays from continental weathering (Odin and Fröhlich, 1988). That said, authigenic clay formation has been empirically observed in nearshore settings around tropical deltas (*e.g.* Rude and Aller, 1994), and Michalopoulos and Aller (1995) showed the plausibility of replicating such processes in laboratory experiments. More recently, field isotope studies have rejuvenated interest in reverse weathering processes (Rahman et al., 2016, 2017; Dunlea et al., 2017; Ramos et al., 2018; Bernhardt et al., 2020) suggesting the significance of authigenic clay formation and reverse weathering for oceanic elemental budgets.

Over the last decade, interest in using lithium (Li) and its isotopes (^{7}Li and ^{6}Li) as a tracer of weathering processes has risen. Because of the long residence time of Li in the ocean, seawater Li isotopes (as recorded by foraminifera) archive global changes occurring at the Earth surface, such as continental weathering (Hathorne and James, 2006; Misra and Froelich, 2012). Reverse weathering, also, has been proposed as a strong control on the Li isotope composition (expressed as δ^7Li relative to standard reference material L-SVEC: δ^7Li (‰) = $(\frac{(^7Li/^6Li)Sample}{(^7Li/^6Li)L\text{-}SVEC} - 1) \times 1000$) of the ocean (Misra and Froelich, 2012; Li and West, 2014). For instance, the steady-state mass balance model of Misra and Froelich (2012) invokes a fractionation of 16‰ (Δ^7Li = δ^7Li$_{seawater}$ − δ^7Li$_{authigenic\text{-}sediments}$) associated with reverse weathering in the ocean. However, such a fractionation has not yet been experimentally verified. A number of experimental studies have addressed the behaviour of Li and its isotopes during the alteration of igneous rocks/minerals, focussing primarily on (1) the effect of both low-temperature seafloor and high-temperature hydrothermal alteration of oceanic basalts (Seyfried

et al., 1984; Berger et al., 1987, 1988; James et al., 2003; Millot et al., 2010); and (2) the partitioning of Li between fluids and solids during silicate weathering on the continents (Pistiner and Henderson, 2003; Vigier et al., 2008; Wimpenny et al., 2010, 2015; Verney-Carron et al., 2011; Hindshaw et al., 2019; Pogge von Strandmann et al., 2019). These studies have shown that in low-temperature environments clay minerals readily take up Li from surrounding fluid with a preference for ^{6}Li (correspondingly, resulting in the enrichment in ^{7}Li of the fluid). This incorporated Li can be hosted at exchangeable sites or chemically bonded into the structural sites, with incorporation into structural sites being the predominant driver of isotopic fractionation toward the enrichment of ^{6}Li in the solid (Vigier et al., 2008; Pogge von Strandmann et al., 2019; Hindshaw et al., 2019).

A limited number of studies have investigated the Li chemical and/or isotope behaviour during sediment-seawater interaction (Zhang et al., 1998; Pogge von Strandmann et al., 2008; Jones et al., 2012). In the experiments of Zhang et al. (1998), fast adsorption of seawater Li onto clay mineral surfaces was associated with preferential uptake of ^{6}Li with fractionation between seawater and solids of 28‰ (seawater-vermiculite) and 21‰ (seawater-kaolinite). However, the experimental procedure of Zhang et al. (1998) was not well documented, and the robustness of the reported isotope measurements has since been questioned (Chan et al., 2006). Jones et al. (2012) conducted a series of experiments consisting of the partial dissolution of riverine/estuarine sediments (derived from Icelandic basalts) in seawater. In these experiments, immersion of riverine sediments in seawater removed a significant amount of Li from the fluid (>70%), but unfortunately Li isotopic fractionation associated with this drawdown was not measured. The field observations of Pogge von Strandmann et al. (2008) on Icelandic estuaries draining basaltic terrains do however indicate that both Li concentration ([Li]) and δ^7Li of riverine particulate materials derived from continental weathering increase rapidly upon arrival at the river estuary. The authors attribute this behaviour to the formation of secondary minerals

4

following the mixing of river waters with seawater. However, the exact mechanism driving this change in particle [Li] and δ^7Li upon entry in the estuary is unidentified. Thus if Li isotopes are to be used as a quantitative constraint on global reverse weathering, a better mechanistic understanding of Li isotope fractionation during processes relevant to the reverse weathering (*e.g.* detrital suspended matter dissolution, Li adsorption onto sediments, and authigenic clay formation) is needed. To fill this gap, we conducted a series of experiments investigating Li isotope fractionation during interaction between seawater and kaolinite which is a typical component of terrigenous sediment material.

2. Materials and methods

2.1 Materials and experiments

Three sets of experiments were conducted at Géosciences Environnement Toulouse (GET), with each set investigating the influence of one particular process (or set of processes) relevant to reverse weathering: (1) far-from-equilibrium dissolution of detrital clays in seawater; (2) the adsorption of Li onto detrital clays; (3) close-to-equilibrium interaction between detrital clays and seawater. In these experiments, to control the chemistry of the reactive solution, and to minimize any effect of biological activity, synthetic open-ocean seawater was used in all experiments. This artificial seawater (ASW), with an ionic strength (I) of $I = 0.7$ M, was synthesised largely following Kester et al. (1967), with some modifications (see Table. 1).

Kaolinite was used as representative material of detrital clays produced by continental weathering and delivered by rivers to the ocean. Poorly crystallized kaolinite (reference KGa-2) from Washington County (Georgia, USA) was supplied by the Source Clay Repository of the Clay Minerals Society (its surface properties are described in Schroth and Sposito, 1997). The Li content and isotope composition of untreated KGa-2 kaolinite ([Li]$_{solid}$ = 95.94 µg/g, δ^7Li = -0.38 ± 0.72 ‰, 2 s.d, n=12) were determined at the Institut de Physique du Globe de

Paris (IPGP) using an Inductively coupled plasma-Quadruple-Mass spectrometer (ICP-Q-MS) and a Thermo Fisher Neptune Plus MC-ICP-MS after acid digestion of powdered aliquots of the solids in HF-HNO$_3$. The specific surface area of the kaolinite powders, as determined by nitrogen adsorption using the Brunauer-Emmet-Teller (BET) method at GET laboratory, was 22.75 ± 5 % m^2/g.

In experiment (1), designed to study far-from-equilibrium clay dissolution, 20.5 g of the KGa-2 powder were immersed in 501.5 g of Li-free ASW at a constant pH value of 2.7, which allowed the experiment to remain at far-from-equilibrium conditions, and prevented the precipitation of any secondary phases. Seven solution samples were taken periodically over the course of the reaction (~28 days), to measure the change in Li, Al and Si concentrations and δ^{7}Li.

In experiment (2), designed to characterize Li adsorption onto detrital kaolinite, the KGa-2 powder was first carefully rinsed 12 times with Milli-Q water (18.2 MΩ·cm) to remove most of the Li located at exchangeable sites or adsorbed at the crystal edges. A suspension made of ~1g of this water-rinsed kaolinite and 30 ml of aqueous solution pre-equilibrated with the same treated kaolinite powder was mixed for several hours in 50 ml PP centrifuge tubes using a tube rotator before Li addition. The aqueous solutions were either ASW or a pure NaCl solution (with the same Na concentration as ASW). Between 71 and ~2,700 μmol/kg of dissolved Li (in the form of LiCl; δ^{7}Li = -6.20 ± 0.01 ‰, 2 s.d, n=2) was subsequently added to the suspensions and the pH was adjusted to the desired value by addition of small amounts of 1 M NaOH. Each suspension was mixed for 30 minutes to 6 days at a ~constant 20°C temperature and then centrifuged at a speed of 6,500 rpm to separate the aqueous solution from the solid. Sample solutions were collected, filtered with 0.2-μm porosity syringe filters and acidified with distilled HNO$_3$ for Li isotope and chemical analyses, and the remaining solution volume used for the pH measurement. The Li partition coefficient between the solid and the

fluid (K_d) was calculated according to Equation 1 below, where m_{Li-ads} and m_{Li-aq} correspond to the mass of Li adsorbed on the solid surface and the mass of Li in solution (m_{Li-ads} was determined from the difference between the initial and final (m_{Li-aq}) aqueous [Li]) and m_{kaol} and m_{sln} designate the corresponding mass of kaolinite and aqueous solution, respectively.

$$K_d = \frac{(m^{Li-ads}/m^{kaol})}{(m^{Li-aq}/m^{sln})} \tag{1}$$

Experiments (3) aimed to investigate the interaction between detrital material and seawater at close-to-equilibrium conditions. Experimental ASW solution was first doped with Li using an ICP standard solution (δ^7Li_{aq}=52.83 ± 0.28 ‰, 2 s.d) to approximately seawater Li concentration ([Li]$_{aq}$ ~25.9 µmol/kg, or ~180 ppb), and its pH was adjusted using NaOH and HCl to pH =8.3. Importantly, this initial ASW solution was devoid of Si and Al, such that only the dissolution of solids was able to provide those elements required for formation of authigenic phases. In this experiment, 20.0 g of KGa-2 powder was immersed in 500.4 g of Li-doped ASW solution. Sampling started 1 day after immersion, with 16 samples taken over the course of the experiment for elemental and Li isotopes analyses. Periodically and after each sample collection, the pH was measured and re-adjusted up to pH~8.4-8.5 using 1M NaOH as required.

Experiments (1) and (3) were conducted in polypropylene (PP) beakers hermetically sealed with PVC lids and rubber O-rings to avoid external contamination and to reduce the effects of evaporation. The solutions were continuously mixed using either a Teflon propeller driven by an overhead stirrer or a suspended Teflon-coated magnetic bar attached to a fish-clip (Fig. 1). Before sampling, the stirring system was stopped and the solid in the reactor allowed to settle for about 20 minutes. Fluid aliquots ranging from 3 to 25 ml were sampled using a weighed, clean syringe attached to a 0.2-µm pore-size filter. The sampled mass was determined via the mass difference of the syringe before and after sampling. Part of the sampled mass was acidified by adding 1 drop of distilled HNO$_3$ and stored for chemical analyses, while the other part was kept for Li isotope measurements. The pH of the aqueous solution was measured *in*

situ by inserting a glass combination electrode inside the reactor through an opening made through the lid for this purpose, while the aqueous solution was mixed. The electrode was calibrated against NIST-certified buffers, and as such pH measurements in this study are reported on the NBS-scale and denoted "pH_{NBS}" hereafter (cf. Millero et al., 1993). Although determination of pH in high ionic strength seawater solutions with electrodes calibrated in low ionic strength buffers may introduce systematic measurement error, this effect is unlikely when viewed in the context of the pH range studied (Dickson, 1984; Millero et al., 1993).

2.2 Fluid chemical and isotopic analyses

The concentrations of dissolved Al and Si were measured via Inductively Coupled Plasma Optical Emission Spectrometry (ICP-OES) at the GET laboratory in Toulouse, using a set of calibration standards prepared with the same matrix used for the experiments. The detection limits were determined to be 0.18 and 0.04 µmol/kg of solution ($\mu mol/kg_{sln}$) for Al and Si, respectively. Additional analyses were conducted via atomic absorption spectrometry (AAS) on selected samples to monitor the possible concentration change of the other cations dissolved in ASW (K, Mg, and Ca). The analytical uncertainty for all the analyzed elements were lower than 2 %.

Measurements of Li concentration and isotope composition were conducted at IPGP. All samples were re-dissolved in 0.5 N HNO_3 and measured by Inductively Coupled Plasma Quadrupole Mass Spectrometry (ICP-Q-MS, Agilent 7900), calibrated using a set of standards with concentrations ranging from 0 to 28.81 $\mu mol/kg_{sln}$ (0-200 ppb). The detection limit ranged from 0.14 to 1.44 $nmol/kg_{sln}$ (1-10 ppt) depending on operational conditions. The analytical uncertainty was normally below 2% but could reach up to ~8% for samples with Li concentrations < 0.14 $\mu mol/kg_{sln}$ (1 ppb).

8

Prior to Li isotope composition measurements of the aqueous solutions, a double-step separation protocol (details in supplementary materials, Table S1) was performed in order to separate Li from the sample matrix. In the first step, a 0.5-ml sample aliquot containing 20 ng of Li in 1 N HNO_3 was loaded onto a 1-ml column (BioRad, AG50W–X12, 200–400 μm mesh) followed by 4 ml of 1 N HNO_3. In the second step, the eluate of the previous columns was again loaded onto the same (but pre-washed) column and then eluted with 16 ml of 0.2 N HNO_3. The last 8 ml of the elution volume were collected for Li measurement. During each separation session, five reference materials were routinely processed together with samples to check for the quality of this protocol. The Li isotope composition of purified samples was measured at IPGP using a Thermo Fisher Neptune Plus MC-ICP-MS using 10^{11}-ohms amplifiers. Six samples (exp. 2) were measured at the German Research Centre for Geosciences (GeoForschungsZentrum GFZ, Potsdam) using a Thermo Neptune Plus MC-ICP-MS and 10^{11}-ohms amplifiers. L-SVEC solution was used as a bracketing standard to correct for instrumental mass fractionation, and repeat measurement of the pure Li standard solution IRMM-016 was used to monitor the instrumental stability. Analysis of five known reference materials (Table. S2), NASS-6 (δ^7Li=30.89 ± 0.48 ‰, 2 s.d, n=7), BHVO-2 (δ^7Li=4.35 ± 0.18 ‰, 2 s.d, n=5), SRM-2709a (δ^7Li=-0.68 ± 0.56 ‰, 2 s.d, n=5), TILL-1 (δ^7Li=6.38 ± 0.46 ‰, 2 s.d, n=6), and JB-2 (δ^7Li=4.38 ± 0.56 ‰, 2 s.d, n=7) yielded values in agreement with previously reported values (*e.g.* Weynell et al., 2017; Kuessner et al., 2020). The analytical uncertainty of δ^7Li in this study is 0.56 ‰, which is obtained from the greatest standard deviation of reference material measurements.

For samples from experiment (1), Li concentrations (0.61 to 1.03 μmol/kg$_{sln}$) were much lower than in seawater (~25.93 μmol/kg$_{sln}$) and the corresponding matrix/Li ratios were ~25 to 42 times greater than seawater, making the separation of Li from the matrix impossible with the method described above. Therefore, the samples were split into several aliquots

(maximum=12) and processed in parallel through the first step of the protocol. Then, eluates were paired and mixed (such that the number of aliquots was halved), and processed through the same first step of Li separation again. The same procedure was repeated until all initial aliquots were combined into one eluate, then the second step was processed. Such a separation procedure was tested using seawater (NASS-6), and the obtained results ($\delta^7Li = 30.86 \pm 0.11$ ‰, 2 s.d, n=2) are in good agreement with previously reported values (*e.g.* Kuessner et al., 2020).

2.3 Solid micro-characterization

Kaolinite samples were analysed before and after the experiments using a JSM 7800F Prime-EDS (JEOL, Ltd.) scanning electron microscope (SEM) at the Castaing Micro-characterization Center in Toulouse to examine the main morphological features of the reacted solids and detect any mineralogical change due to solid-solution interactions.

Lithium bonding environment was characterized for solids from the adsorption experiment (exp. 2) using Nuclear Magnetic Resonance (NMR) at the research unit of CEMHTI (Conditions Extrêmes et Matériaux: Haute Température et Irradiation; CNRS, Orléans). Solid samples from the two adsorption runs that showed the highest amounts of Li sorption onto the kaolinite surface in NaCl and ASW solutions, KL-17 (78.3 µg/g; NaCl solution) and KL-18 (44.3 µg/g; ASW), were analysed together with one sample of unwashed KGa-2 powder and one of KGa-2 rinsed with Milli-Q water (see above). ^7Li Magic Angle Spinning (MAS) NMR spectra were acquired on a Bruker AVANCE III spectrometer (750 MHz – 17.6 T) at a Larmor frequency of 291.5 MHz and a spinning speed of 30 kHz. Around 2000 scans were made with a recycling delay of 10s, ensuring complete relaxation of the signal. ^7Li chemical shifts were referenced relative to a 1 M LiCl solution.

2.4 Thermodynamic calculations

Aqueous solutions' speciation and saturation states with respect to relevant secondary phases were calculated from measured aqueous concentrations and pH using the geochemical code PHREEQC v. 3.3 (Parkhurst and Appelo, 2013) and its "LLNL" thermodynamic database. Activity coefficients for dissolved species were calculated using the extended Debye–Hückel equation. The saturation state of the aqueous solution relative to the solid phases of interest is expressed by the saturation index: $SI = Log_{10}(Q/K_{sp})$, where Q defines the ion activity product of the species involved in the hydrolysis of the mineral and K_{sp} is its solubility product value. It must be noted that, given the uncertainty of pH measurements and the possible limitations inherent in the activity coefficient model here used, we do not claim to provide a precise determination of the thermodynamic parameters related to the composition of our ASW solutions. Rather, the results of these thermodynamic calculations should be considered qualitative estimates of such parameters.

3. Results

3.1 Kaolinite dissolution in Li-free, acidic seawater

The results of this experiment (1) are summarized in Table 2 and illustrated in Fig. 2. After an initial rapid dissolution phase with preferential Al release relative to Si, kaolinite dissolution proceeded stoichiometrically, while the fluid remained undersaturated with respect to kaolinite or to any tested Al-Si secondary phase. The absence of newly-formed secondary phases was also confirmed by SEM observations of both fresh and reacted solid KGa-2 powders that showed no discernible difference in appearance (Figure S1). Aqueous Li concentrations, below the detection limit during the first hours of reaction, continuously increased with time, with the light Li isotope being preferentially released into solution (Fig. 2). A preferential release of Li relative to Si during the entire course of the experiment was also observed (Fig. 3). Isotopically, whereas bulk kaolinite exhibits an initial δ^7Li_{solid} value of -0.38

‰, the composition of the first aqueous sample (after ~7 days of experiment) was $\delta^7Li_{aq}=$ -16.61 ± 0.11‰. With time the δ^7Li_{aq} only slightly decreased, reaching a value of -19.03 ± 0.20‰ after 28 days of reaction.

3.2 Li adsorption on kaolinite

The results of Li sorption experiments on kaolinite powders are reported in Table 3. It can be seen that the exact nature of the background electrolyte (0.41 M NaCl or ASW) and the exposure time had little effect on the value of the Li partition coefficient K_d as defined by Eq. (1). Most K_d observed values are between 0 and 5.7, except one large K_d value (28.2) obtained from a run in which the initial $[Li]_{aq}$ (71.1 µmol/kg) was significantly lower than in the other runs (> 490 µmol/kg). Adsorbed Li concentrations ranges from 0.2 up to 64 µg/g, and are positively correlated with fluid pH (Fig. S2a). Li partition coefficients exhibited a slight increase at alkaline pH for solutions used in this study which have relatively low Li aqueous concentrations (≤ 2.7 mmol/kg$_{sln}$). Also, a linear increase in the amount of Li adsorbed as a function of initial $[Li]_{aq}$ was observed at $9.6 < pH_{NBS} < 11.0$ for Li concentrations varying between 71 and 2,700 µmol/kg$_{sln}$ (Fig. S2b).

Four fluid samples were analysed to determine the isotopic composition of adsorbed Li. These data (Table 4) show that the lighter Li isotope is preferentially adsorbed on the kaolinite surface, with a fractionation between kaolinite surface and aqueous solution ($\Delta^7Li_{ads-sln}$) of between -24.2 and -25.8 ‰ (excepting a single value at -14.6 ‰ which we consider to be an analytical artefact of unidentified origin).

The ^7Li NMR spectra of initial non-treated kaolinite, initial kaolinite rinsed in deionized water and kaolinite recovered from Li adsorption runs KL-17 and KL-18 are shown in Fig. 4. It can be seen that removal of exchangeable or weakly adsorbed Li by water rinsing resulted in a displacement of ^7Li chemical shift of -0.07 ppm (from -0.10 to -0.17 ppm) whereas Li adsorption on water-rinsed kaolinite (runs KL-17 and KL-18) provoked a displacement of the

^{7}Li peak in the opposite direction from -0.17 to -0.08 ppm, which may reflect the adsorption of Li more weakly bounded than Li substituted in kaolinite octahedral sites (^{7}Li peak shift < -0.17 ppm).

3.3 Kaolinite interaction with Si- and Al-free and Li-doped seawater at pH$_{NBS}$ = 8.3 ± 0.1

Aqueous Si concentration in experimental seawater increased sharply at the beginning of the run and approached a steady state (~ 28 μmol/kg$_{sln}$) after 166 days of reaction (Table 5, Fig. 5). At the same time Al concentration remained almost constant, with values ≤ 1 μmol/kg and close to the analytical detection limit. Solution Li concentration (26 μmol/kg at t = 0) rapidly decreased during the course of the reaction attaining a final concentration of 5.5 μmol/kg$_{sln}$, indicating Li uptake by solids. About 80% of the Li initially present in solution was thus removed during the experiment, corresponding to a partition coefficient K$_d$ between kaolinite and solution of 89.6. This Li removal was accompanied by a strong relative enrichment of the heavy Li isotope in the solution. During the first 39 days, δ^{7}Li$_{aq}$ increased rapidly from 52.8 to 75.4 ‰, and then at a slower rate over the following ~120 days, up to 80.2 ‰. Throughout the experiment, solution pH decreased somewhat (Table 5), although NaOH was added in order to maintain relatively stable conditions. PHREEQC calculations indicate that the reacting fluid became undersaturated with respect to kaolinite within a few days, but strongly supersaturated with respect to saponites (SI > 2.0) and mildly supersaturated or close to equilibrium with respect to calcite, gibbsite, and illite (Fig. 6). SEM and Energy-dispersive X-ray (EDX) spot analyses of the solid recovered at the end of the run, however, do not indicate any difference in morphology and chemical composition compared to the initial kaolinite (Fig. S3).

4. Discussion

4.1 Lithium isotope fractionation during kaolinite dissolution in seawater

Significant kaolinite dissolution occurred during the experiment in which kaolinite was dissolved in Li-free seawater at pH_{NBS} ~2.7 (Exp. 1). A preferential release of Al and Li over Si was observed (Fig. 2a and 3) in accordance with kaolinite dissolution promoted by proton-Al^{3+} exchange reactions (Oelkers et al., 1994; Devidal et al., 1997). Li release, approximately stoichiometric relative to Al (Li/Al = 1.5-1.8×10^{-3} mol/mol), was accompanied by a fast and strong enrichment of the solution in the lighter Li isotopes (δ^7Li_{aq} = -16.61 ‰ after 7 days, Fig. 2b) followed by a much weaker variation with time (δ^7Li_{aq} = -19.03 ‰ after 28 days) leading to significant isotope fractionation between the final aqueous solution and the remaining solid, $\Delta^7Li_{sln-kaol}$ = -18.68 ‰. Since kaolinite dissolution in experiment 1 is stoichiometric and our thermodynamic calculations suggest the reacting solution is undersaturated with respect to any secondary mineral, the observed enrichment of the solution in ^6Li cannot be explained by the precipitation of new solid phases. Instead, lithium isotope fractionation must have occurred during dissolution. According to mass balance calculations, 0.17 % of the Li contained in kaolinite was released, whereas only 0.11 % of Si was removed from the solid. The limited fraction of Li leached from the starting solid thus results in an insignificant variation of the Li isotopic composition of the solid over the duration of the experiment (~0.03 ‰).

Two different mechanisms could be invoked to explain the observed Li isotope fractionation during early-stage dissolution of kaolinite in seawater: kinetic effects and Li release from different kaolinite sites. Significant kinetic isotope fractionation is known to occur during solid precipitation/dissolution because the rates of desolvation/solvation of light metal isotopes – and thus the breaking rate of light Me-O bonds in the crystal lattice – are faster than those of heavy metal isotopes. Such an effect can in particular result in isotope fractionation during early-stage dissolution (*e.g.* Weiss et al., 2014). Based on molecular dynamics

simulation of the exchange rate of water molecules in metal isotopes hydration spheres, Hofmann et al. (2012) proposed that the maximum value of the kinetic fractionation factor, α_{kin}, could be approximated by:

$$\alpha_{kin} = \frac{k_{wex,i}}{k_{wex,j}} = \left(\frac{m_i}{m_j}\right)^{-0.049} \tag{2}$$

where $k_{wex,i}$ stands for the water exchange rate constant for the isotope i of mass m_i. Application of Eq. (2) to the $^7Li/^6Li$ system yields a maximum value of the kinetic fractionation factor equal to 0.9925 ($\Delta^7Li_{fluid-solid}$ = -7.5 ‰). This value is consistent with the findings of Verney-Carron et al. (2011) who reported a maximum kinetic fractionation, $\Delta^7Li_{fluid-glass}$, of -5.4 ‰, during the early stage of dissolution of a Li-enriched synthetic basaltic glass where secondary mineral precipitation did not occur. However, the faster breaking of ^6Li-O bonds described by Eq. 2 (maximum value -7.5 ‰) cannot alone explain the enrichment of the fluid in ^6Li observed in the present study ($\Delta^7Li_{sln-kaol}$ = -18.68 ‰).

Alternatively, in exp. (1) Li could have been released from specific crystallographic sites. In kaolinite, Li (a) likely substitutes for Al in octahedral sites, (b) is adsorbed as bidendate inner-sphere complexes on edge octahedra, and to a lesser extent, (c) is located in interlayer sites (Miranda-Trevino and Coles, 2003; Fairén et al., 2015). A part of the Li released to the solution could derive from Li bound to exchangeable sites and/or edge octahedral sites. However, both the stoichiometric Li release relative to Al and the strong enrichment of the solution in ^6Li during initial non-stoichiometric kaolinite dissolution strongly suggests that Li was removed from the AlO_6 octahedral sites where it substitutes for Al, rather than from interlayer sites. These sites are known to be characterized by a strong enrichment in ^6Li relative to the bulk solid. For example, in the layered silicates synthesized by Hindshaw et al. (2019), Li in octahedral sites is about 15 and 21‰ lighter than in the bulk solid and at the exchangeable sites, respectively.

Therefore, our preferred interpretation for the observed large Li isotope fractionation during kaolinite dissolution is the preferential release of [6]Li from octahedral sites, although the impact of a faster breaking rate of [6]Li-O bonds compared to [7]Li-O cannot be discounted. It is important to notice that in our experiment, kaolinite dissolution was performed in artificial seawater of 0.7 M ionic strength. However, the results of this experiment should also apply to solutions of much lower ionic strength, like those characterizing most continental waters, because in our experiment kaolinite dissolution proceeded at far-from-equilibrium conditions where no sorption or backward reactions (regulated by the composition of the solution) could occur.

4.2 Li isotope fractionation during adsorption at the kaolinite surface

The δ^7Li values of solution equilibrated with pre-washed KGa-2 in exp. (2) were all higher than that of the initial solution, which is consistent with Li isotopic fractionation during adsorption onto kaolinite. Metal adsorption onto kaolinite surfaces is thought to occur mainly at edge sites (Brady et al., 1996, 1998). Adsorption onto kaolinite edge sites is pH-dependent and particularly predominant when pH is above 7 (Liu et al., 2018), as in our experiments. The observed [7]Li chemical shift of 0.09 ppm (from -0.17 to -0.08 ppm, Fig. 4) in the NMR analysis of solids from exp. (2) is also consistent with the presence of adsorbed Li onto octahedral AlO_6 sites exposed at kaolinite edges. Therefore, we attribute the observed isotope shift of the solutions during exp. (2) to Li adsorption onto kaolinite edge sites inducing preferential uptake of light Li.

The δ^7Li of the adsorbed fraction, as calculated by isotope mass balance, ranged from -28.30‰ to -19.46‰, corresponding to fractionation factors between solid and fluid between 0.9745 and 0.9856 ($\Delta^7Li_{ads-sln}$ = -25.8 to -14.6 ‰). The measured range of fractionation is relatively large because of the anomalous value found for the experiment KL-18: a replicate of

experiment KL-16 but with higher initial Li concentration (2710 *vs.* 493 µmol/kg$_{sln}$). If this likely erroneous value is not considered, the mean Li isotope fraction resulting from Li sorption is $\Delta^7Li_{ads-sln}$ = -24 ‰, a value comparable to those determined by Zhang (2001) from experiments where natural seawater from the Gulf of Mexico was left to interact with kaolinite (-21 ‰), and to that obtained in the present study during the interaction of kaolinite with seawater at pH$_{NBS}$~8.3 (-21‰, see § 4.3). Li in solution is coordinated with 4 water molecules as a tetrahedral aqua ion. The adsorbed Li onto edge sites can be as either outer-sphere complexes (the coordination number of Li remains as 4) or inner-sphere complexes (the coordination number of Li becomes 6) (cf. Liu et al., 2018; Hindshaw et al., 2019). The isotope fractionation of adsorption is mainly associated with the change of coordination number. Therefore, the strong enrichment in ^6Li of adsorbed lithium confirms that Li increases its coordination number from 4 to 6 upon adsorption and is bounded to kaolinite AlO$_6$ edge sites in the form of octahedral inner-sphere surface complexes.

4.3 Li isotope fractionation during kaolinite-seawater interaction

In our experiment of seawater-kaolinite interaction at pH$_{NBS}$ 8.3, net dissolution of kaolinite is indicated by increasing dissolved Si concentration through time. No significant release of Al to the solution was observed (Fig. 5a) in contrast to the dissolution of KGa-2 in acidified seawater at far-from-equilibrium conditions (Fig. 2a), suggesting the rapid formation of secondary Al-bearing phases, including clay minerals or their amorphous precursors. Although little evidence for the formation of secondary phases was seen under SEM (Fig. S3), thermodynamic calculations (Fig. 6) suggest that the solution is supersaturated with respect to several secondary phases, in particular Mg-saponite, Na-montmorillonite and gibbsite. As shown in Fig. 5b, this experiment was characterized by a significant removal of Li (~80%) from the initial solution, accompanied by a strong enrichment of ^7Li in the fluid (~25‰ increase

in dissolved δ^7Li). This is in agreement with previously published results (Zhang et al., 1998; Millot and Girard, 2007) showing that clays preferentially incorporate light Li isotopes. Two main mechanisms can explain the Li uptake and isotopic fractionation observed during our experiment: (1) the adsorption of Li at kaolinite edge octahedral sites as shown by the previous experiment and, (2) the direct Li incorporation in the lattice of newly formed secondary phases, such as saponites.

Depending on the process that controls Li uptake by the solid, the change in Li aqueous isotopic composition in a batch experiment can be described according to either (a) "closed system" equilibrium, in which the Li adsorbed to or incorporated in the solids remains available to isotopic exchange during the progress of the reaction, or (b) Rayleigh distillation, in which the Li adsorbed at the solid surface or incorporated in the precipitating solid is prevented from further isotopic exchange with the solution. The evolution of the Li isotope composition of the aqueous solution for these two behaviours can be expressed as:

(a) Closed system equilibrium: $\delta^7Li_{aq}(t) = \delta^7Li_{aq}(t=0) - 1000 \times (\alpha-1) \times F$ (3a)

(b) Rayleigh distillation: $\delta^7Li_{aq}(t) = \delta^7Li_{aq}(t=0) + 1000 \times (\alpha-1) \times ln(1-F)$ (3b)

where $\delta^7Li_{aq}(t=0)$ and $\delta^7Li_{aq}(t)$ are the isotopic compositions of the initial solution and of the same solution at time t, respectively. In both equations, α is the fractionation factor between the solid and the solution; and F stands for the fraction of Li removed from the solution (Eq. 3c below), where $[Li]_{aq}(t=0)$ and $[Li]_{aq}(t)$ are the Li concentrations of initial solution and the same solution at time t.

(c) $F = 1 - \dfrac{[Li]aq(t)}{[Li]aq(t=0)}$ (3c)

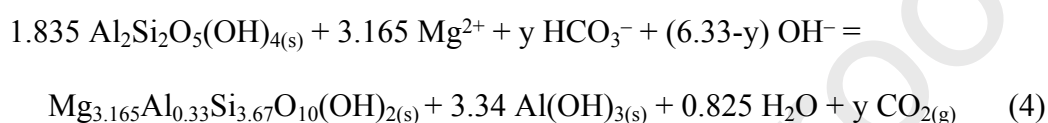To test the ability of either mechanism to describe the Li isotope fractionation observed in our experiment, in Fig. 7 we have plotted $\delta^7Li_{aq}(t)$ as a function of F, which can be calculated from the Li concentration and solution volume at time t. A single linear relationship (Eq. 3a) yielding a fractionation factor α of 0.968 ($\Delta^7Li_{sol-fluid} = -32‰$) provides a good fit to the entire dataset

but does not satisfactorily explain the δ^7Li_{aq} change observed during the first part of experiment 3 (Fig. 7a). Since δ^7Li_{aq} increases non-linearly during this initial stage and such a fractionation (-32‰) is much larger than any Li isotope fractionation factor yet reported, we discount simple "closed system" behaviour. Alternatively, the trend can be reasonably fitted by Eq. (3b) (Fig. 7b). However, we note that a systematic deviation between the experimental data and the best fit Rayleigh distillation function exists for high F values (later stage of the experiment; Fig. 7b). These observations lead us to conclude that the observed evolution of the fluid Li isotopic composition is the result of a two-stage scenario (Fig. 7b). In the early stage the Li removal from the fluid follows a Rayleigh fractionation process with an estimated fractionation factor of 0.979 ($\Delta^7Li_{sol-fluid}$ = -21‰), indicating a one-way transfer of material from the fluid to the solid. In the second stage the evolution of the Li isotopic composition follows a closed-system equilibrium fractionation with a two-way transfer of material to and from the solid, and a fractionation factor equal to 0.981 ($\Delta^7Li_{sol-fluid}$ = -19‰). Note, the transition to the second reaction stage requires the introduction of a new coordinate reference where the removal of dissolved Li is represented by F', with $F' = 0$ at the beginning of the new stage. This two-phase scenario yields very similar Li isotope fractionation factors for the Rayleigh and closed-system stages, which are in good agreement with the fractionation values reported for Li sorption onto kaolinite and vermiculite by Zhang (2001) and onto kaolinite in our own experiment (section 4.2). Additionally, the two-step scenario model (root-mean-square-error (RMSE) = 0.79) better fits the measured data than the closed-system-only model (RMSE=1.0).

Mechanistically, we suggest these two stages in isotope fractionation behaviour reflect two subsequent reactions controlling the Li removal from the fluid. First, Li is rapidly taken up by the precipitating secondary Al-bearing phases such as saponites and gibbsite during the first 7 days of reaction, preventing any isotopic re-equilibration of Li between the solid and the aqueous solution. Subsequently, much slower uptake by secondary phases and/or adsorption at

the solid surfaces produces a constant isotope exchange between the two phases. Thus in this interpretation of the data, *both* co-precipitation in secondary phases and adsorption play an important role in the Li removal from the fluid and its isotopic fractionation.

The rapid precipitation of secondary phases is consistent with the fast pH and Li concentration decreases observed during the early stage of the reaction (0-7 days) (Table 5, Fig. 5) and can be exemplified by the following reaction describing the formation of Mg-saponite and gibbsite during kaolinite interaction with seawater:

$$1.835 \, Al_2Si_2O_{5}(OH)_{4(s)} + 3.165 \, Mg^{2+} + y \, HCO_3^- + (6.33\text{-}y) \, OH^- =$$

$$Mg_{3.165}Al_{0.33}Si_{3.67}O_{10}(OH)_{2(s)} + 3.34 \, Al(OH)_{3(s)} + 0.825 \, H_2O + y \, CO_{2(g)} \qquad (4)$$

First, we note that such reaction consumes OH⁻ ions and therefore acidifies the solution, thereby providing an explanation as to why regular addition of NaOH was necessary to keep a relatively constant pH during the experiment. In addition, this reaction leads to the consumption of alkalinity and to the release of CO_2. As such it is typical of the reverse weathering pathway initially invoked by Mackenzie and Garrels (1966) to illustrate the idea that cations released from the continents by chemical weathering of rocks (and the CO_2 taken up in the process) could eventually be re-sequestered by the neoformation of sedimentary clays in the ocean (and the CO_2 released).

When comparing the Li isotope fractionation resulting from our experiment with that provided by Zhang (2001) for Li sorption on kaolinite, it must be noted that the author derived his value using a Rayleigh fractionation model without taking into account the possible formation of secondary phases. Apart from Li, no information was provided in Zhang (2001)'s study on the evolution of the solution pH and chemical composition, but it is likely that in this experiment the reported Li fractionation factor at least partially reflects Li incorporation in secondary phases.

5. Implications and conclusions

Besides providing experimental constraints on the fundamental properties of the Li isotope system (K_d and isotope fractionation factors), the results of our experimental study have important implications for the global Li cycle as well as its isotope mass balance.

First, the fact that both early-stage kaolinite dissolution and Li adsorption onto kaolinite entail significant Li isotope fractionation is noteworthy because kaolinite, among other clay minerals, is a major constituent of soils and, as a result, can greatly affect the isotopic composition of the Li dissolved in soil water. Although Li isotope data on soil solutions are scarce, available data (Lemarchand et al., 2010; Pogge von Strandmann et al., 2012) show an enrichment in ^6Li with depth in soils' upper layers, which is consistent with the preferential release of ^6Li observed in this study during kaolinite dissolution. Obviously, our experimental results were obtained in very acidic conditions (pH < 3) compared to those usually encountered in soil water, but we contend that a similar Li fractionation during kaolinite dissolution should be expected when mildly acidic rain water, undersaturated with respect to clay minerals, percolate through the topmost soil horizons. During rain storms, this low δ^7Li signal could even propagate all the way to the river outflow. In most cases, however, this effect cannot dominate the long-term, weighted-average export of dissolved Li from catchments, which is generally characterized by a relatively high δ^7Li value (*e.g.* Huh et al., 1998; Dellinger et al., 2015; Henchiri et al., 2016; Hindshaw et al., 2019; Murphy et al., 2019), because clay formation and associated ^6Li uptake outweighs the release of ^6Li by clay dissolution (Dellinger et al., 2015). We hypothesize that soil and river dissolved Li isotopes recorded during a flood event could show transient, preferential release of ^6Li through the partial dissolution of kaolinite, thereby producing a negative excursion in δ^7Li in the river water. More generally, such far-from-equilibrium conditions might be encountered in catchments where hydrological flow paths are rapid, or when water-mineral contact times are short, like in small catchments affected by

landslides. In addition to kaolinite dissolution, the strong Li isotope fractionation during adsorption inferred from our experiments might contribute significantly to short-term variations in the Li isotope signature of soil and river water through fluctuations in the solid-to-water ratios in soils and rivers.

The results of our study also have implications on the global, longer-term Li cycle. There is probably a large range of possible reactions occurring when riverine material interacts with seawater or sediment pore-water, but the type of reactions that we identified in this study and that occur relatively rapidly (in a couple of weeks in the conditions of our experiments) will act to make the Li isotopic composition of the ocean heavier, even at the very early stage of diagenesis. The Li isotope fractionation observed during two of our experiments (Li adsorption onto kaolinite and interaction between kaolinite and seawater at pH_{NBS} ~8.3) suggest that the detrital clay minerals transported to the ocean by rivers may have a significant impact on the Li chemical and isotopic composition of the ocean, as suggested by Misra and Froelich (2012) and Li and West (2014). With a total flux of suspended matter transported annually by the world rivers to the ocean of 19 Gt (Milliman and Farnsworth, 2013), if one assumes that 10% of this flux (a conservative estimate for the global kaolinite+smectite content of the continental detrital flux to the oceans; see Guyot et al. (2007) and Pinet et al. (2019) for the case of the Amazon) is composed of clay minerals exhibiting a Li partition coefficient equal to 42, (an intermediate value between the values observed in our experiment on kaolinite adsorption (K_d = 89.6; see § 3.2) and those reported by Zhang (2001)), the amount of aqueous Li that can be removed from the ocean (taking the modern value for Li concentration in seawater of 180 μg/kg) is equal to 2.1×10^9 moles/yr. In comparison, the annual flux of dissolved Li brought into the ocean by rivers is equal to 10×10^9 moles (Gaillardet et al., 2003; Huh et al., 1998; Misra and Froelich, 2012). Therefore, provided that this Li initially adsorbed is later locked into newly formed phases, as observed in our experiment of interaction between kaolinite and seawater at

22

pH$_{NBS}$ = 8.3, this could result in a significant long-term sink of oceanic, river-derived dissolved Li. Furthermore, the impact of Li scavenging by river suspended matter on the ocean Li isotopic composition can be approximated by the following mass balance equation:

$$\delta^7Li_{sw}(initial) = f \times \delta^7Li_{sw}(scav) + (1-f) \times \delta^7Li_{sw}(final), \qquad (5)$$

where $\delta^7Li_{sw}(initial)$ and $\delta^7Li_{sw}(final)$ stand for seawater Li isotopic composition before and after Li scavenging by clay minerals, respectively, and f and $\delta^7Li_{sw}(scav)$ represent the Li fraction and Li isotope composition of seawater Li scavenged by clay minerals, respectively. With an ocean mass of 1.36×10^{21} kg and a seawater Li concentration of 26 µmol/kg$_{sln}$, the total amount of Li in seawater is equal to 3.53×10^{16} moles. Given an annual flux of Li removed from the ocean by suspended matter equal to 2.1×10^9 moles (hence $f = 5.9 \times 10^{-8}$), and $\Delta^7Li_{kaol-sw} \sim -20$‰ (as indicated by both experiments of kaolinite adsorption onto kaolinite and kaolinite-seawater interaction at pH$_{NBS} \sim 8.3$), the Li isotopic composition of the ocean could be enriched by this process by about 1.2 ‰ over a period of 1 Myr, assuming that the process of Li incorporation into the detrital material is irreversible over these time scales. Froelich and Misra (2012) reported that the present seawater Li isotopic composition is about 9‰ heavier than the late Paleocene (~60 Ma). The isotope effect caused by detrital clays on seawater δ⁷Li, as predicted from our experimental results, is therefore a plausible cause for the Cenozoic rise in seawater δ⁷Li, showing that the impact of detrital clay-seawater interactions cannot be neglected on geological time scales (Li and West, 2014).

Finally, with regard to the secular evolution of the seawater δ⁷Li, the fractionating mechanisms investigated in this study bring qualitative arguments to the importance of reverse weathering reactions for controlling the Cenozoic increase of seawater δ⁷Li reported by several authors. Some authors have recently proposed that during the Cenozoic, the development of river floodplains and coastal plains could have helped neoformation of clay minerals on land and contributed to an increase in the riverine δ⁷Li (Dellinger et al., 2015; Pogge von

Strandmann and Henderson, 2015). Alternatively, our experiments suggest that with increasing erosion fluxes due to uplift over the Cenozoic, an increase of detrital clay material supply to the ocean could enhance the neoformation of diagenetic minerals in marine environments, and therefore increase seawater δ^7Li globally (Li and West, 2014). The balance between the importance of neoformation of new clay minerals in floodplains and reverse weathering reactions is still uncertain but both must be considered in interpreting the observed oceanic δ^7Li curve. Overall, our experiments therefore confirm the potential of Li isotope marine archives as tracers of both continental weathering and marine reverse weathering.

References

Berger G., Schott J. and Loubet M. (1987) Fundamental processes controlling the first stage of alteration of a basalt glass by seawater: an experimental study between 200 and 320 C. *Earth Planet. Sci. Lett.* **84,** 431-445.

Berger G., Schott J. and Guy C. (1988) Behavior of Li, Rb and Cs during basalt glass and olivine dissolution and chlorite, smectite and zeolite precipitation from seawater: experimental investigations and modelization between 50 and 300 C. *Chem. Geol.* **71,** 297-312.

Bernhardt A., Oelze M., Bouchez J., von Blanckenburg F., Mohtadi M., Christl M. and Wittmann H. (2020) 10Be/9Be ratios reveal marine authigenic clay formation. *Geophys. Res. Lett.* **47,** e2019GL086061.

Brady P. V., Cygan R. T. and Nagy K. L. (1996) Molecular Controls on Kaolinite Surface Charge. *Journal of Colloid and Interface Science* **183,** 356-364.

Brady P. V., Cygan R. T. and Nagy K. L. (1998) Chapter 17 - Surface Charge and Metal Sorption to Kaolinite. *in* Adsorption of Metals by Geomedia: Variables, Mechanisms, and Model Applications, Everett A. Jenne *Ed.*, 371-382, Academic Press.

Chan L., Leeman W. P. and Plank T. (2006) Lithium isotopic composition of marine sediments. *Geochem. Geophys. Geosyst.* **7,** Q06005.

Dellinger M., Gaillardet J., Bouchez J., Calmels D., Louvat P., Dosseto A., Gorge C., Alanoca L. and Maurice L. (2015) Riverine Li isotope fractionation in the Amazon River basin controlled by the weathering regimes. *Geochim. Cosmochim. Acta* **164,** 71-93.

Devidal J., Schott J. and Dandurand J. (1997) An experimental study of kaolinite dissolution and precipitation kinetics as a function of chemical affinity and solution composition at 150°C, 40 bars, and pH 2, 6.8, and 7.8. *Geochimica et Cosmochimica Acta* **61,** 5165-5186.

Dickson A. G. (1984) pH scales and proton-transfer reactions in saline media such as sea water. *Geochimica et Cosmochimica Acta* **48,** 2299-2308.

Dunlea A. G., Murray R. W., Ramos D. P. S. and Higgins J. A. (2017) Cenozoic global cooling and increased seawater Mg/Ca via reduced reverse weathering. *Nature Communications* **8,** 844.

Fairén A. G., Losa-Adams E., Gil-Lozano C., Gago-Duport L., Uceda E. R., Squyres S. W., Rodríguez,J.Alexis P., Davila A. F. and McKay C. P. (2015) Tracking the weathering of basalts on Mars using lithium isotope fractionation models. *Geochem. Geophys. Geosyst.* **16,** 1172-1197.

Gaillardet J., Viers J. and Dupré B. (2003) Trace elements in river waters. *Treatise on geochemistry* **5,** 605.

Guyot J. L., Jouanneau J. M., Soares L., Boaventura G. R., Maillet N. and Lagane C. (2007) Clay mineral composition of river sediments in the Amazon Basin. *CATENA* **71,** 340-356.

Hathorne E. C. and James R. H. (2006) Temporal record of lithium in seawater: A tracer for silicate weathering? *Earth Planet. Sci. Lett.* **246,** 393-406.

Henchiri S., Gaillardet J., Dellinger M., Bouchez J. and Spencer R. G. M. (2016) Riverine dissolved lithium isotopic signatures in low-relief central Africa and their link to weathering regimes. *Geophys. Res. Lett.* **43,** 4391-4399.

Hindshaw R. S., Tosca R., Goût T. L., Farnan I., Tosca N. J. and Tipper E. T. (2019) Experimental constraints on Li isotope fractionation during clay formation. *Geochim. Cosmochim. Acta* **250,** 219-237.

Hofmann A. E., Bourg I. C. and DePaolo D. J. (2012) Ion desolvation as a mechanism for kinetic isotope fractionation in aqueous systems. *Proc. Natl. Acad. Sci. USA* **109,** 18689-18694.

Huh Y., Chan L., Zhang L. and Edmond J. M. (1998) Lithium and its isotopes in major world rivers: implications for weathering and the oceanic budget. *Geochim. Cosmochim. Acta* **62,** 2039-2051.

Isson T. T. and Planavsky N. J. (2018) Reverse weathering as a long-term stabilizer of marine pH and planetary climate. *Nature* **560,** 471.

James R. H., Allen D. E. and Seyfried W. (2003) An experimental study of alteration of oceanic crust and terrigenous sediments at moderate temperatures (51 to 350 C): Insights as to chemical processes in near-shore ridge-flank hydrothermal systems. *Geochim. Cosmochim. Acta* **67,** 681-691.

Jones M. T., Pearce C. R. and Oelkers E. H. (2012) An experimental study of the interaction of basaltic riverine particulate material and seawater. *Geochim. Cosmochim. Acta* **77,** 108-120.

Kester D. R., Duedall I. W., Connors D. N. and Pytkowicz R. M. (1967) Preparation of artificial seawater. *Limnol. Oceanogr.* **12,** 176-179.

Kuessner M. L., Gourgiotis A., Manhès G., Bouchez J., Zhang X. and Gaillardet J. (2020) Automated Analyte separation by Ion Chromatography using a Cobot Applied to Geological Reference Materials for Li Isotope Composition. *Geostand Geoanal Res* **44**, 57-67

Lemarchand E., Chabaux F., Vigier N., Millot R. and Pierret M. (2010) Lithium isotope systematics in a forested granitic catchment (Strengbach, Vosges Mountains, France). *Geochimica et Cosmochimica Acta* **74,** 4612-4628.

Li G. and West A. J. (2014) Evolution of Cenozoic seawater lithium isotopes: Coupling of global denudation regime and shifting seawater sinks. *Earth Planet. Sci. Lett.* **401,** 284-293.

Liu Y., Alessi D. S., Flynn S. L., Alam M. S., Hao W., Gingras M., Zhao H. and Konhauser K. O. (2018) Acid-base properties of kaolinite, montmorillonite and illite at marine ionic strength. *Chemical Geology* **483,** 191-200.

Mackenzie F. T. and Garrels R. M. (1966) Chemical mass balance between rivers and oceans. *Am. J. Sci.* **264,** 507-525.

Michalopoulos P. and Aller R. C. (1995) Rapid Clay Mineral Formation in Amazon Delta Sediments: Reverse Weathering and Oceanic Elemental Cycles. *Science* **270,** 614-617.

Millero F. J., Zhang J., Fiol S., Sotolongo S., Roy R. N., Lee K. and Mane S. (1993) The use of buffers to measure the pH of seawater. *Marine Chemistry* **44,** 143-152.

Milliman J. D. and Farnsworth K. L. (2013) *River discharge to the coastal ocean: a global synthesis.* Cambridge University Press,

Millot R. and Girard J. (2007) Lithium isotope fractionation during adsorption onto mineral surfaces. In *International Meeting on Clays in Natural & Engineered Barriers for Radioactive Waste Confinement, Lille, France.*

Millot R., Scaillet B. and Sanjuan B. (2010) Lithium isotopes in island arc geothermal systems: Guadeloupe, Martinique (French West Indies) and experimental approach. *Geochim. Cosmochim. Acta* **74,** 1852-1871.

Miranda-Trevino J. C. and Coles C. A. (2003) Kaolinite properties, structure and influence of metal retention on pH. *Applied Clay Science* **23,** 133-139.

Misra S. and Froelich P. N. (2012) Lithium Isotope History of Cenozoic Seawater: Changes in Silicate Weathering and Reverse Weathering. *Science* **335,** 818-823.

Murphy M. J., Porcelli D., Pogge von Strandmann, Philip AE, Hirst C. A., Kutscher L., Katchinoff J. A., Mörth C., Maximov T. and Andersson P. S. (2019) Tracing silicate weathering processes in the permafrost-dominated Lena River watershed using lithium isotopes. *Geochim. Cosmochim. Acta* **245,** 154-171.

Odin G. and Fröhlich F. (1988) Chapter C3 Glaucony from the Kerguelen Plateau (Southern Indian Ocean). In *Developments in Sedimentology*. Elsevier, pp. 277-294.

Oelkers E. H., Schott J. and Devidal J. (1994) The effect of aluminum, pH, and chemical affinity on the rates of aluminosilicate dissolution reactions. *Geochimica et Cosmochimica Acta* **58,** 2011-2024.

Parkhurst D. L. and Appelo C. (2013) Description of input and examples for PHREEQC version 3--A computer program for speciation, batch-reaction, one-dimensional transport, and inverse geochemical calculations. **6-A43,** US Geological Survey

Pinet S., Lartiges B., Martinez J. and Ouillon S. (2019) A SEM-based method to determine the mineralogical composition and the particle size distribution of suspended sediment. *International Journal of Sediment Research* **34,** 85-94.

Pistiner J. S. and Henderson G. M. (2003) Lithium-isotope fractionation during continental weathering processes. *Earth Planet. Sci. Lett.* **214,** 327-339.

Pogge von Strandmann Philip AE, James R. H., van Calsteren P., Gíslason S. R. and Burton K. W. (2008) Lithium, magnesium and uranium isotope behaviour in the estuarine environment of basaltic islands. *Earth Planet. Sci. Lett.* **274,** 462-471.

Pogge Von Strandmann, Philip AE, Opfergelt S., Lai Y., Sigfússon B., Gislason S. R. and Burton K. W. (2012) Lithium, magnesium and silicon isotope behaviour accompanying weathering in a basaltic soil and pore water profile in Iceland. *Earth Planet. Sci. Lett.* **339,** 11-23.

Pogge von Strandmann, Philip AE and Henderson G. M. (2015) The Li isotope response to mountain uplift. *Geology* **43,** 67-70.

Rahman S., Aller R. and Cochran J. (2016) Cosmogenic 32Si as a tracer of biogenic silica burial and diagenesis: Major deltaic sinks in the silica cycle. *Geophys. Res. Lett.* **43,** 7124-7132.

Rahman S., Aller R. and Cochran J. (2017) The missing silica sink: revisiting the marine sedimentary Si cycle using cosmogenic 32Si. *Global Biogeochem. Cycles* **31,** 1559-1578.

Ramos D. P. S., Morgan L. E., Lloyd N. S. and Higgins J. A. (2018) Reverse weathering in marine sediments and the geochemical cycle of potassium in seawater: Insights from the K isotopic composition (41K/39K) of deep-sea pore-fluids. *Geochim. Cosmochim. Acta* **236,** 99-120.

Rude P. D. and Aller R. C. (1994) Fluorine uptake by Amazon continental shelf sediment and its impact on the global fluorine cycle. *Continental Shelf Research* **14,** 883-907.

Schroth B. K. and Sposito G. (1997) Surface charge properties of kaolinite. *Clays Clay Miner.* **45,** 85-91.

Seyfried W., Janecky D. and Mottl M. (1984) Alteration of the oceanic crust: implications for geochemical cycles of lithium and boron. *Geochim. Cosmochim. Acta* **48,** 557-569.

Sillen L. G. (1967) The ocean as a chemical system. *Science* **156,** 1189-1197.

Verney-Carron A., Vigier N. and Millot R. (2011) Experimental determination of the role of diffusion on Li isotope fractionation during basaltic glass weathering. *Geochim. Cosmochim. Acta* **75,** 3452-3468.

Vigier N., Decarreau A., Millot R., Carignan J., Petit S. and France-Lanord C. (2008) Quantifying Li isotope fractionation during smectite formation and implications for the Li cycle. *Geochim. Cosmochim. Acta* **72,** 780-792.

Weiss D. J., Boye K., Caldelas C. and Fendorf S. (2014) Zinc Isotope Fractionation during Early Dissolution of Biotite Granite. *Soil Science Society of America Journal* **78,** 171-179.

Weynell M., Wiechert U. and Schuessler J. A. (2017) Lithium isotopes and implications on chemical weathering in the catchment of Lake Donggi Cona, northeastern Tibetan Plateau. *Geochimica et Cosmochimica Acta* **213,** 155-177.

Wimpenny J., Gíslason S. R., James R. H., Gannoun A., Pogge Von Strandmann, Philip AE and Burton K. W. (2010) The behaviour of Li and Mg isotopes during primary phase dissolution and secondary mineral formation in basalt. *Geochim. Cosmochim. Acta* **74,** 5259-5279.

Wimpenny J., Colla C. A., Yu P., Yin Q., Rustad J. R. and Casey W. H. (2015) Lithium isotope fractionation during uptake by gibbsite. *Geochim. Cosmochim. Acta* **168,** 133-150.

Zhang L., Chan L. and Gieskes J. M. (1998) Lithium isotope geochemistry of pore waters from Ocean Drilling Program Sites 918 and 919, Irminger Basin. *Geochim. Cosmochim. Acta* **62,** 2437-2450.

Zhang L. (2001) Lithium Isotope Geochemistry of Marine Sediments. Ph.D. thesis, Louisiana State University Historical Dissertations and Theses. 257.